ELSEVIER

Parts-per-billion (ppb) selective iodine sensors leveraging metal–organic framework nanoenvironment

Arun S. Babal [1,†], Samraj Mollick [1,†], Waqas Kamal [2], Steve Elston [2], Alfonso A. Castrejón-Pita [2], Stephen M. Morris [2], Jin-Chong Tan [1,*]

[1] Multifunctional Materials and Composites (MMC) Laboratory, Department of Engineering Science, University of Oxford, Parks Road, Oxford OX1 3PJ, United Kingdom
[2] Department of Engineering Science, University of Oxford, Parks Road, Oxford OX1 3PJ, United Kingdom

Ultra-sensitive and highly selective iodine gas sensors play a crucial role during the nuclear radiation leak for a timely detection and mitigation of pollution, ensuring the safety of a vast number of operators and subsequent integrity of the facility. Herein, we rationally designed a metal–organic framework (MOF) that exhibits an outstanding performance with an almost billionfold enhancement in the electrical response due to its optimized hydrophobicity, which allows the easy migration of iodine molecules through the channels and the presence of suitable interaction sites, temporarily anchoring the target molecule for ultra-trace sensing. The prototype sensor tested in demanding environments demonstrates its high selectivity, ultra-trace parts per billion (ppb)-level sensitivity, good reversibility, and a very fast response time even at high frequencies compared to existing adsorbents, including commercially available materials. Further, the iodine sensing at the atomic level was studied in detail by measuring the electrical response of a single crystal and, the optimal thickness of the MOF layer was identified for an industrially-viable prototype sensor by using inkjet printing. In a wider perspective, we propose a general strategy for engineering electrically efficient sensing materials that will enable the construction of high-sensitivity iodine sensors targeting a safe and sustainable future.

Keywords: Iodine sensor; Metal–organic framework; Transient impedance; Guest–host interactions; Inkjet printing

Introduction

Nuclear is the backbone of greenhouse gas-free energy, providing up to 10% of the global energy demand [1]. To meet the ever-increasing energy demand of society, it is considered the most promising alternative source over fossil fuels due to its high energy density, low operational cost, and low greenhouse gas emission, which leads to a reduced carbon footprint [2,3]. Despite these advantages, in developed countries, the age of nuclear energy starts to fade away due to the concerns associated with the emission of radioactive gases during nuclear accidents and fuel reprocessing that has severe long-term impacts on both the environment and human health [4]. Mostly, radionuclides are emitted in the form of gases and can enter our food chain through contaminated air, which deposits these radioactive molecules on agricultural soil and into drinking water supplies. One of the major gases of concern is iodine, with its isotopes including ^{131}I (half-life: 8 days) and ^{129}I (half-life: 1.7 million years), which adversely impact human metabolism and are a major cause of thyroid cancer [5–8]. Conventional iodine sensors have certain shortcomings that must be tackled, i.e. low sensitivity, poor selectivity, short-term reusability, and sensing only at higher temperatures [9–12]. To address these long-standing chal-

* Corresponding author.
E-mail address: Tan, J.-C. (jin-chong.tan@eng.ox.ac.uk)
† These authors contributed equally to this work.

lenges, a more effective technology needs to be developed to selectively detect the ultra-trace levels of radionuclides in the case of a nuclear breach or fuel preprocessing facilities to maintain a hazard-free working environment and to ensure safety for the wider community.

Metal-organic frameworks (MOFs) are ideal candidates for sensing studies, which have started to gain the attention of the scientific community due to their high surface area, tunable pore size, design versatility as well as with their exceptional combination of structural, thermal, and chemical robustness. MOF materials can be tailor-made to incorporate specific interaction sites to selectively accommodate target gas molecules [13–16]. Currently, optical techniques are widely studied in the field of gas-phase sensing in MOFs, but for industrial applications, a direct electric response far outweighs it due to the real-time highly compact setup with low-cost manufacturing, and high readability, and better assimilation with modern electronics [11,17–19]. However, electrical sensing of non-polar gases such as I_2 remains an immense challenge due to the shortfall of effective materials to afford practical designs. In this regard, a material with a judicious combination of optimal hydrophobicity and interaction sites could be an ideal candidate for ultra-trace (ppb level) I_2 detection in the gas phase, but this has yet to be achieved.

Herein, a series of prototype sensors was prepared by drop-casting, in-situ growth of single crystals, or inkjet printing MOFs, on a platform of interdigitated electrodes (IDEs) to fabricate a highly selective and ultra-trace (ppb-level sensitivity) gas-phase iodine sensor. A ppb-level high sensitivity was realized in a MOF material through a rational tuning of the optimal hydrophobicity and guest–host interaction sites (Scheme 1). In the presence of iodine, a very fast reversible millionfold enhancement in alternating current (AC) signals and a remarkable billionfold enhancement in direct current (DC) was achieved for the electrical response of the prototype sensor due to its high adsorption capacity. Here, the optimal hydrophobicity allows adsorption of the non-polar iodine gas molecules and suitable interaction sites selectively trap them to the host framework, accomplishing a ppb-level sensitivity. Furthermore, the gas phase ultra-high selectivity of the MOF material was tested by studying the cyclic electrical response in different volatile organic compounds (VOCs) and water-saturated environments, in addition to the optimal thickness of the MOF layers on the prototype sensor to standardize the system for potential industrial application. Finally, a room temperature electrical response study was conducted to simulate a real-time sensing application.

Results and discussion

The prototype sensor platform consists of interdigitated comb-like electrode (IDE) structures on a glass substrate coated with an insulating polymeric film. For the qualitative comparison between the sensors, the electrical response (impedance, capacitance, and phase angle) from the empty IDE was measured in addition to their response toward the iodine gas, which remained unchanged as shown in Fig. 1. Later, thin films of different MOFs were prepared on the sensors *via* various methods i.e., drop casting, in-situ single crystal growth, and inkjet printing (controlled layered deposition) and then dried in the presence of inert N_2 gas (see SI Section 1.2). Powder X-ray diffraction (PXRD) was carried out for all the MOFs to confirm their crystalline structure, before characterizing the electrical response from the prototype sensors (see Fig. S2). The variance in the electrical response of empty and MOF-deposited sensors was non-existent, which confirms the insulating nature of MOFs (as a low–*k* dielectric). The effect of hydrophilicity, hydrophobicity, and interaction sites of candidate MOF materials on high selectivity and ultra-trace sensitivity toward the specific gas was monitored to study their individual impact, and subsequently those individual parameters are combined to ascertain the final optimized material.

The different prototypical MOFs: MOF-808 and F300 for hydrophilicity, ZIF-11 and ZIF-71 for hydrophobicity, ZIF-65 for its functional nitro-group, and ZIF-68 and ZIF-70 for their interaction site and optimal hydrophobicity, were selected as a sensing material for gas phase detection of I_2 (see Fig. 1(a)–(d) and Figs. S4–S7). MOF-808 is a zirconium-based MOF with an **spn** topology, formed by corner-sharing tetrahedral subunits comprising secondary building units (SBUs) on vertices and linkers on faces [20]. This structure contains two types of pore: one big adamantane-shaped pore with a pseudohexagonal pore window within each tetrahedral tertiary building unit, and a cage within each tetrahedral tertiary building unit. Because of this geometry, each linker unit points directly into a large pore. F300 is a trade name for the Fe-BTC MOF, which is constructed from Fe(III) octahedral trimers connected by benzene-1,3,5-tricarboxylic (BTC) linkers [21]. F300 has a super tetrahedron structure, with big and small pore sizes ranging from 24 to 29 Å. ZIF-11 has an extended 3-D network with a **rho** topology, where each Zn(II) ion is tetrahedrally-coordinated to four nitrogen atoms in benzimidazole (bIm) linkers. The framework is composed of truncated cuboctahedron cages comprising the 8-, 6-, and 4-membered ring windows [$4^{12} \times 6^8 \times 8^6$], where larger cages are linked to smaller openings in the **rho** topology. ZIF-11 has excellent thermal and chemical resistance to water and organic solvents. ZIF-71 also features a **rho** topology, with pore diameters of 16.5–16.8 Å and is constructed by Zn(II) cations bridged by 4,5-dichloroimidazolate (dcIm) linkers. In addition to its four- and six-membered rings (4MR & 6MR) pore apertures, the big cages are connected by eight-membered rings (8MR) with a cage window size of 4.2–4.8 Å [22]. The topology of ZIF-65 is sodalite (**sod**), with pore sizes and window apertures of 10.4 Å and 3.4 Å, respectively. The structure comprises Zn(II) cations connected by nitroimidazole (nIm) linkers. ZIF-68 and ZIF-70 both have the gmelinite (**gme**) topology with large pore channels (10.2 and 15.9 Å in diameter for ZIF-68 and ZIF-70, respectively) penetrated by smaller window apertures (7.5 and 13.1 Å) [23]. These MOFs are composed of an equimolar amount of two distinct linkers, one of which is nIm and the second linker is the unsubstituted imidazole (Im); the incorporation of mixed linkers is crucial for determining different pore sizes and functions. Unlike the other MOFs, which showed a lack of H_2O-induced contribution in the sensor response, the hydrophilic MOFs: MOF-808 and F300 exhibited a significant shift in the electrical response under room conditions in contrast to the empty IDE sensor, suggesting that the high conductivity and polarizability of the H_2O molecules absorbed on the hydrophilic sites of the porous framework greatly influence the sensor perfor-

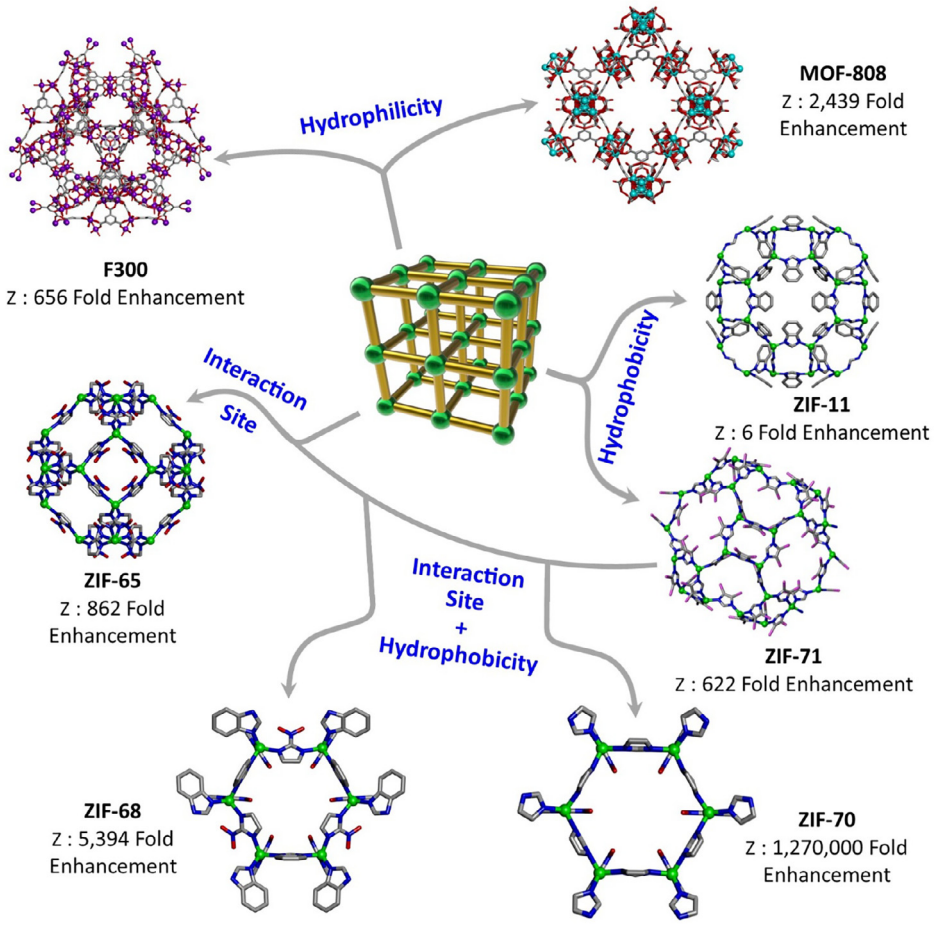

SCHEME 1

Summary of optimal chemical and physical properties to yield highly selective and sensitive MOF for gas phase iodine sensing. The *Z* number denotes the enhancement in the electrical response achieved by each of the MOF structure relative to the "empty" IDE substrate at 4 Hz (i.e. MOF-free IDE as a control sensor).

mance. To evaluate the impact of moisture on the sensor response, F300@IDE was tested at 2 different relative humidity conditions (35 and 46% RH), validating that a higher electrical response is associated with the increasing RH (see Fig. 1(a) & (c) and Fig. S4).

In the presence of iodine gas, the overall sensitivity of hydrophilic prototype MOFs: MOF-808 (mass change of ~50%) and F300 (mass change of ~48%) is a combination of both H_2O and I_2 molecules (present in the MOF pores), decreasing the impedance response further by 656 and 2,439 folds, respectively (see Fig. 1 (f)) and showed a noticeable transition in the phase angle (θ) from −42° (MOF-808) and −37° (F300) to almost 0° at lower frequencies, indicating a transition in electrical response from a capacitive to resistive type (see Fig. 1(d)). The slightly higher sensitivity of F300 MOF over MOF-808 can be ascribed to its higher iodine adsorption capacity (see Fig. 1(e)). The presence of H_2O molecules in the hydrophilic pore negatively affects the inbound target molecules (shrinks the adsorption capacity of the framework) and decreases the overall sensitivity as well as reusability of the sensor devices, rendering them ineffective for the real time gas phase sensing except for application as a humidity sensor. In consideration of these factors and to eliminate the impact of moisture on sensor sensitivity, we selected ZIF-11 and ZIF-71 as a prototype hydrophobic MOF for I_2 sensing, which showed no alterations in the electrical response under ambient conditions (see Fig. S5). Despite the advantages of not being affected by the moisture, the hydrophobicity causes a decrease in the iodine adsorption, which in turn leads to an unwanted lowering of the electrical response of the sensor. Unlike the extreme hydrophobicity of ZIF-11, which brings about a decline in the iodine adsorption (mass change of ~11%), and causes an exceedingly low enhancement in the impedance ratio of only 6-fold; the ZIF-71 framework has a comparatively higher iodine adsorption capacity (mass change of ~27%), enhancing its electrical response to 622-fold, which is comparable with the hydrophilic MOF sensors (see Fig. 1(e) & (f)).

In addition to the characterization of the hydrophilicity and hydrophobicity of the MOF candidates, the interaction sites can also play a key role in the selective capture of the targeted molecules. In this regard, ZIF-65 was chosen to evaluate the impact of interaction sites on iodine adsorption and its electrical sensing response, because it has a nitro-group as part of its linker molecule. The ZIF-65@IDE is unaffected by the presence of moisture, and it adsorbs a notable amount of iodine molecule yielding a mass change of 47% when exposed to the iodine gas (see Fig. 1 (e)). The electron deficient nitro-group acts as an anchor point

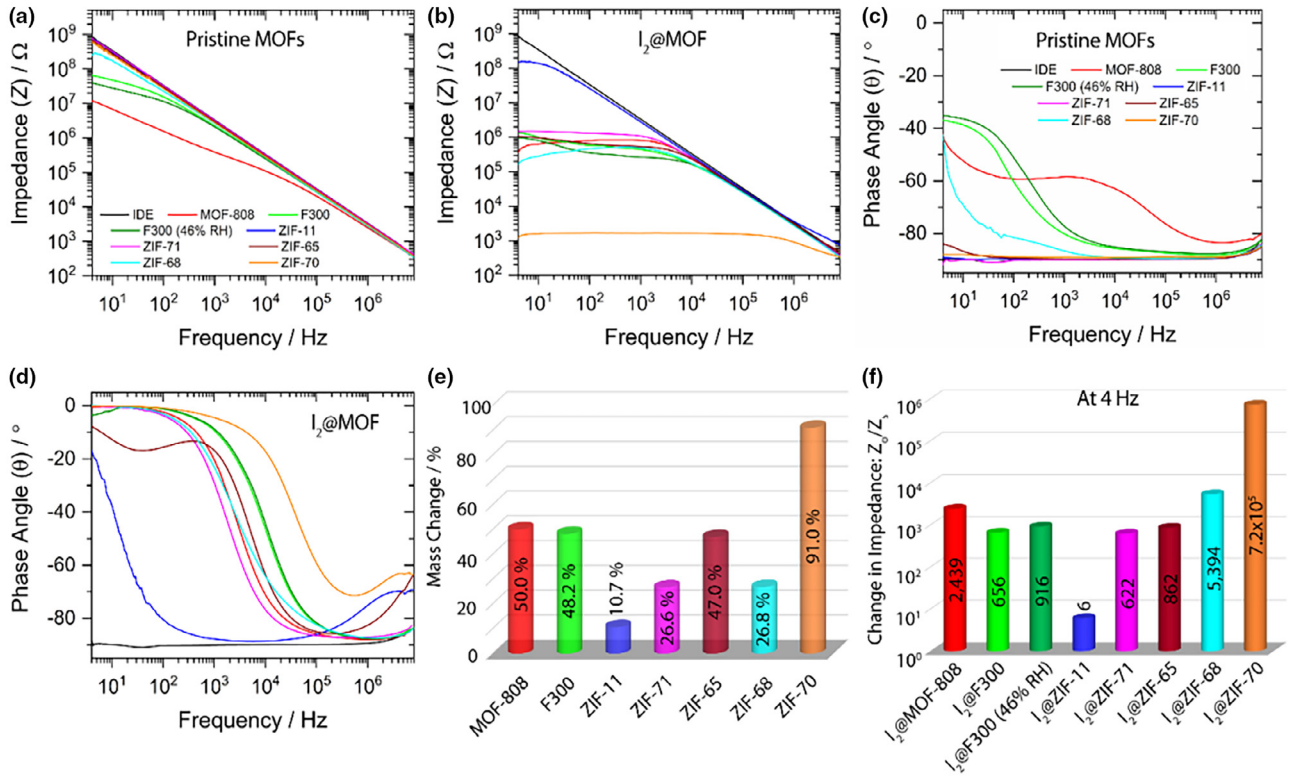

FIGURE 1

Electrical response from the MOF@IDE prototypes at room temperature: before and after iodine adsorption: (a), (b) Impedance signal and (c), (d) phase angle as a function of frequency, respectively. (e) Percentage change in sample mass, and (f) the change in impedance ratio of various MOF structures, after iodine exposure.

for the inbound iodine molecules and partially polarizes them. An increase in the polarization causes a significant rise in the capacitance value (1876% enhancement) as seen in Figs. S8 and S9, which is comparable to the hydrophilic MOFs, where water is highly polarizable. For ZIF-65 MOF, the phase angle showed a slight deviation in the pattern compared to the other tested MOFs, by not showing a complete transition from almost −90° to 0°, when exposed to iodine gas. We reasoned that the effect resulted from the interaction of iodine molecules with the framework, producing a marked 862-fold enhancement in the ratio of impedance values at 4 Hz, which is higher than the values of the hydrophobic MOF ZIF-71 as well as the hydrophilic MOF F300 (see Fig. 1(f)). Collectively, the data obtained from the hydrophilic, hydrophobic, and interaction site-based MOFs indicate that to achieve an ultra-high sensitivity I_2 sensor, the individual properties of MOFs are insignificant. An interaction site-based MOF with optimal hydrophobicity, which is a combination of extreme hydrophobicity and hydrophilicity could be a way forward to harness the MOF potential in the field of electrical sensing for iodine gas detection.

For this purpose, two different prototypical MOFs: ZIF-68 and ZIF-70 were chosen, comprising the same interaction site (nitro-group from 2-nitroimidazole) and different hydrophobicity based on the secondary linker molecule. The hydrophobicity of MOFs was adjusted by varying the secondary linker molecule, from the imidazole (Im) to benzimidazole (bIm) for ZIF-70 and ZIF-68, respectively. The presence of the additional benzene ring in the structure makes the ZIF-68 framework more hydrophobic compared with the ZIF-70 structure and can provide further validation to the optimal hydrophobicity requirement theory for the ultra-high electrical gas sensing of non-polar gases. The hydrophobic linker molecule protects the highly polar water molecules by impeding their negative impact on sensor performance, while the electron deficient nitro-group acts as a temporary anchor point for the inbound iodine molecules, by partially polarizing them causing an overall shift in the structural properties to generate a very high electrical response from the prototype sensors. The iodine adsorption capacity of ZIF-68 MOF (mass change ~27%) was relatively low compared to the ZIF-70 MOF (mass change ~91%), which was a direct result of its higher hydrophobic nature (see Fig. 1(e)). In the presence of iodine gas, the increase in impedance ratio of 5394-fold for ZIF-68 is impressive and indicative of the formation of a percolation network when exposed to a small amount of iodine, albeit this is nowhere near the astonishing increase of 0.73-millionfold in impedance ratio at 4 Hz for ZIF-70, which is an exemplar of an optimal combination of hydrophobicity and interaction site (see Fig. 1(f)). We proposed that the adsorbed iodine provides new and faster charge transfer pathways in the framework causing a decrease in the material impedance. It is well established that at higher iodine concentrations upon adsorption in framework pores, they form an interconnected networks of polyiodides, which decrease the material resistance by providing the charge transfer pathways [24,25]. Likewise, for the other mea-

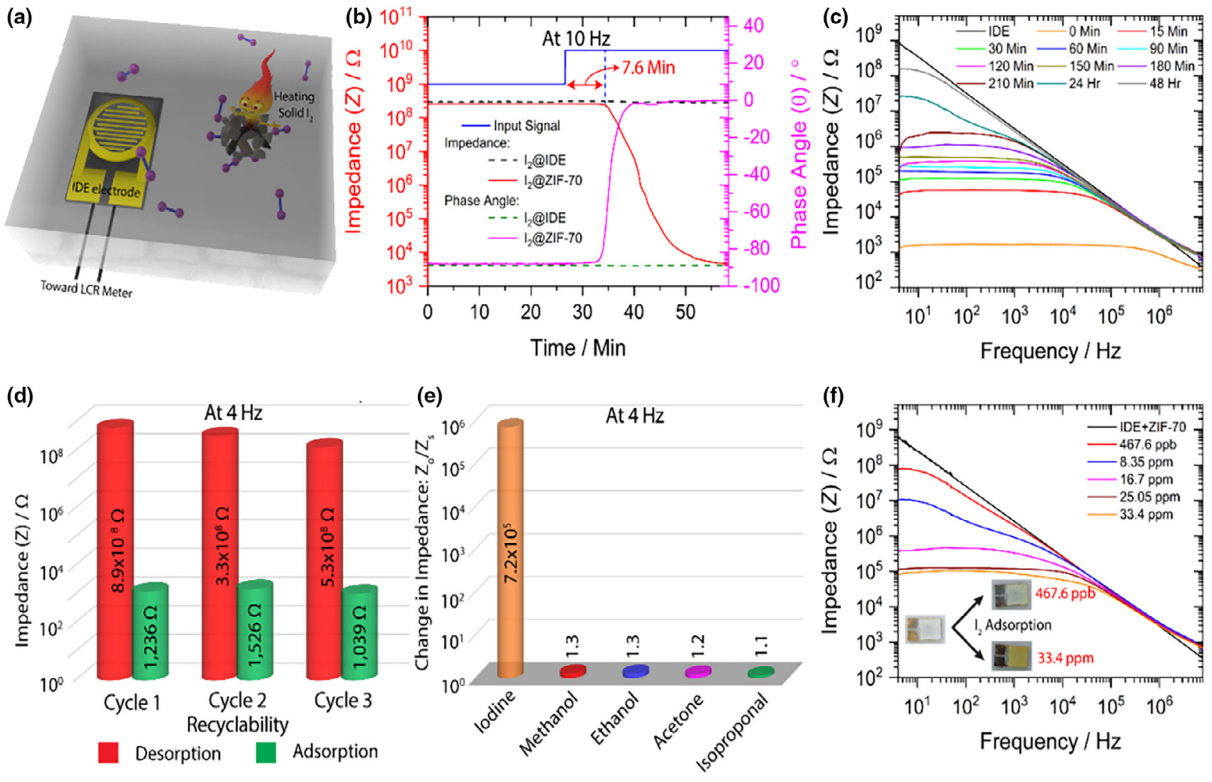

FIGURE 2

Drop-casting of ZIF-70 on an IDE sensor platform for iodine gas sensing: (a) A scheme of real-time iodine sensing setup. (b) Continuous impedance and phase angle measurements as a function of time, during iodine exposure, and (c) the effect of time-dependent iodine desorption on impedance value of ZIF-70@IDE as a function of frequency. (d) Recyclability study of prototype sensor over several adsorption–desorption cycles. (e) The change in impedance ratio of various MOF structures, after iodine exposure. (f) The impedance sensitivity of ZIF-70 prototype sensor at different concentrations of ppb-ppm levels.

surement for ZIF-70 MOF, such as the phase angle transition from −90° to 0° was stable up to $<10^3$ Hz, implying its potential as a frequency-dependent sensor material for iodine gas. From the systematic studies above, it was established that the ZIF-70 MOF, which contains both interaction site and optimal hydrophobicity is the unrivalled candidate, and it should be studied in detail to further optimize the different sample preparation parameters and operational conditions that could impact its gas phase iodine sensing performance.

To confirm whether the location of iodine is inside or outside the framework pore, we conducted a controlled experiment, where the guest is designed to be encapsulated inside the MOF pore. In this context, the ZIF-71 MOF was chosen due to the ease of encapsulation of the triethylamine (TEA) guest molecule inside the pore. From Fig. S10, it is evident that the impedance value of ZIF-71 is much lower compared to that of the guest-encapsulated framework and, it keeps decreasing with increased guest concentration suggesting that the iodine inside the pore plays a major role in reducing the impedance value. So, it can be stated that the electrical response obtained for ZIF-70 is contributed by iodine present both on the MOF surface and inside the pores.

Advancing forward, to reveal the true performance of ZIF-70 MOF, we devised a real-time sensing environment by exposing the prototype sensor to the iodine gas at room temperature and continuously collecting the sensor transient electrical response: impedance and phase angle at 10 Hz frequency as shown in the scheme of Fig. 2(a). The electrical response of an empty IDE sensor (without MOF coating) to iodine was also recorded for comparison, which remained unaffected by the presence of iodine gas. After iodine exposure, it takes 7.6 min to register an electrical response from the prototype sensor, which can be observed in Fig. 2(b). In addition to the iodine adsorption, a time-dependent iodine desorption response from ZIF-70@IDE was also measured at room temperature. It is evident from Fig. 2(c) that, the adsorbed iodine starts to desorb from the framework structure as soon as it is removed from the iodine-rich environment. For the initial first few hours, the desorption rate was much higher, but this decreased as a function of time. After 48 h, most of the iodine had desorbed, causing a significant rise in impedance value, which is closer to the impedance value of iodine-free MOFs, suggesting a disruption in the percolation pathway. To further validate the sensor reversibility, the impedance measurement was carried out for ZIF-70 at 4 Hz for several iodine adsorption (at 70 °C for 30 min)-desorption (at 70 °C for overnight) cycles, which remained quite stable and shows a highly reversible electrical response (see Fig. 2(d)). It further strengthens the case of adopting ZIF-70 as a sensing material. Another important factor that can severely impact the sensor performance is its selectivity toward the targeted molecule. For this purpose, we investigated hydrophilic MOF F300, hydrophobic MOF ZIF-71, ZIF-65 MOF with interaction site and ZIF-70

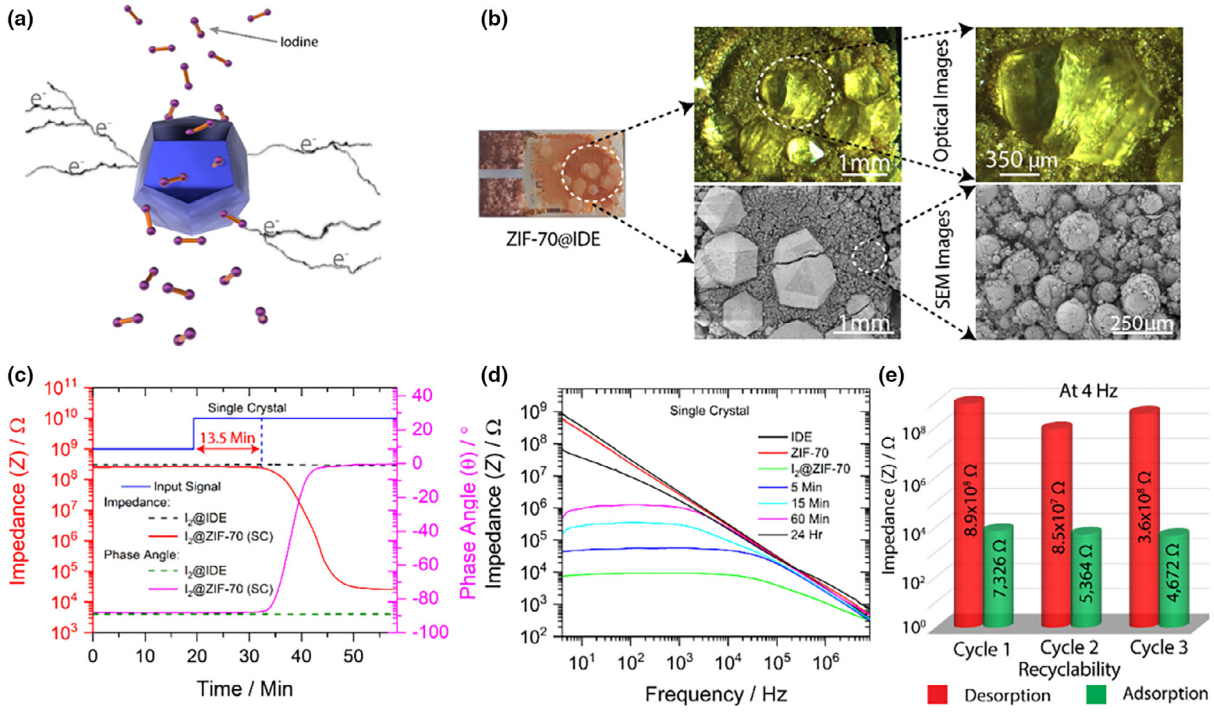

FIGURE 3

Single crystal-based (SC) iodine gas sensing of ZIF-70@IDE: (a) A scheme of increase in electron conduction in single crystal resulted from iodine adsorption. (b) Optical and SEM images of ZIF-70 crystals grown on an IDE sensor platform, observed at different magnifications. (c) A real-time measurement of the transient signals of impedance and phase angle at 10 Hz frequency for ZIF-70 crystals, when exposed to iodine gas. (d) A time-dependent desorption study of ZIF-70 crystals. (e) A cyclic adsorption and desorption data to demonstrate the sensor reusability.

with optimal hydrophobic-interaction site, to determine their solvent-dependent sensitivity for practical use.

As shown the Fig. S12, an enclosed chamber was specifically designed to carry out the vapor saturation study. The prototype sensors were first flushed with nitrogen gas to remove moisture content, subsequently the nitrogen flowed through the solvent containing bubbler to form a saturated environment to carry out the electrical measurements. It was clear from Figs. S13 and S14 that, except for ZIF-70 (see Fig. 2(e)), all other MOFs show an enhanced capacitance and impedance at lower frequencies in the presence of common solvent vapors, which will limit the iodine gas sensing under real-world conditions. Furthermore, the sensitivity of a sensor is also a key criterion to evaluate its performance, which is dependent upon the adsorbent gas concentration. In this regard, we performed impedance measurements on ZIF-70 MOF at different iodine concentrations to validate its potential for sensing the ultra-trace amount of I_2 in gas phase, as shown in Fig. 2(f). It was observed that even at a ppb-level concentration the material shows a clear transition from a white appearance to a yellow color, and the impedance change of the ZIF-70 MOF is still significantly higher, which confirms its capability to accomplish ppb-level sensing of iodine gas and further strengthens the case for deploying ZIF-70 as an ideal iodine gas sensing material combining ultra-high sensitivity and excellent selectivity. Additionally, an adsorption–desorption cyclic study of solvent vapor was carried out on ZIF-70@IDE at 10 Hz frequency to confirm the repeatability of the electrical response (see Fig. S15).

For a comprehensive understanding of I_2 gas phase sensing in the ZIF-70 framework structure, we carried out the single-crystal sensing experiments by directly growing large single crystals of ZIF-70 (>200 µm) onto the top surface of IDE sensor chips, as shown in Fig. 3(b). Interestingly, as compared to the drop-casted sensors, the electrical response of the prototype single-crystal (SC) sensor is lower due to the crystal thickness, which delayed the electrical response by extending the I_2 adsorption time. It was further validated by measuring the time-dependent electrical response of the crystals in the presence of I_2 gas, which showed a time lag in registering the response of about 13.5 min compared to the 7.6 min observed for the drop-casted sensor (see Fig. 3(c) *vs.* Fig. 2(b)). The single crystal showed a negligible electrical response under room conditions, which can be attributed to residual solvents trapped in the pores. In the presence of iodine vapor, the single-crystal sensor showed a remarkable increase of 0.12-millionfold in impedance ratio at 4 Hz. It was also observed that the I_2 desorption rate of single crystal is much higher than the drop-casted sensors and can be associated with stress-induced cracks on the crystal surface. It was further supported by the reversibility experiment, in which several adsorption–desorption cycles were carried out and it showed a systemic decline in the impedance of the I_2 adsorbed sensor, suggesting a crack-induced enhancement in iodine adsorption. To the best of our knowledge, we have demonstrated for the first time gas phase sensing using MOF single crystals integrated on an IDE sensor platform with unprecedented sensitivity.

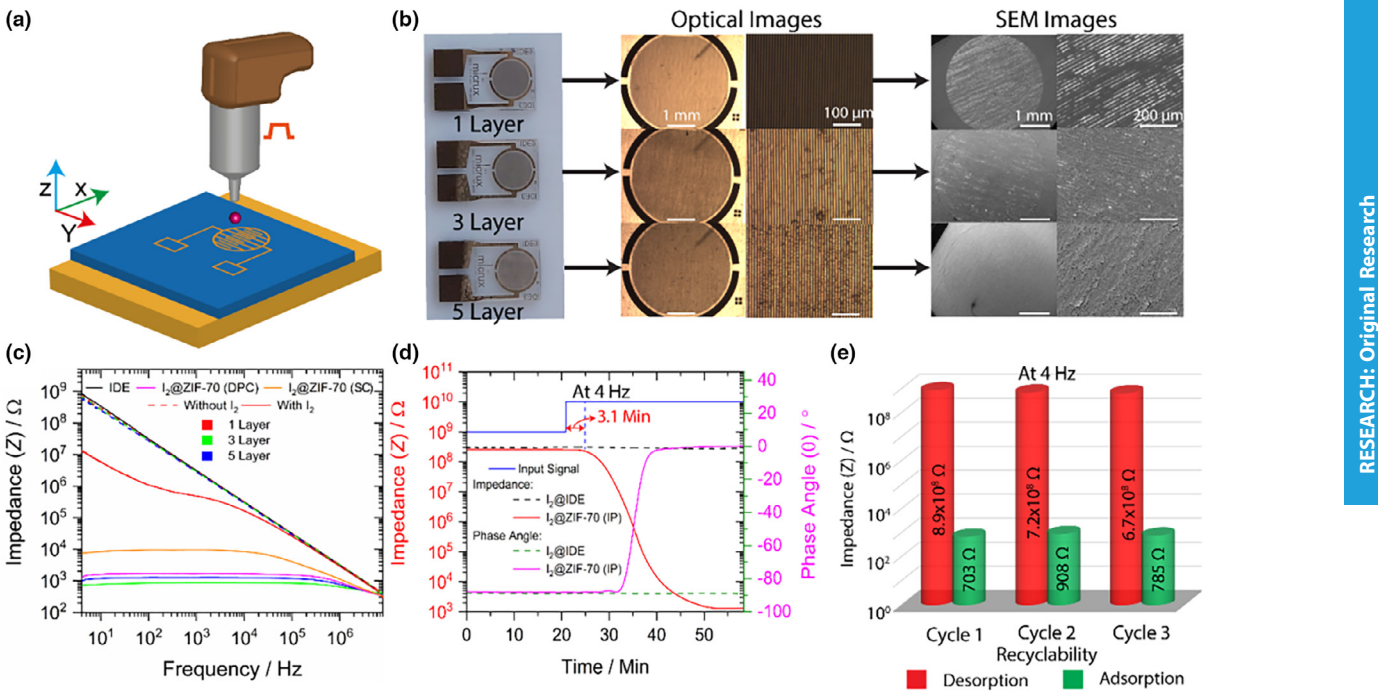

FIGURE 4

Inkjet printing (IP) of ZIF-70 on an IDE sensor platform for iodine gas sensing: (a) An illustration of the inkjet printing technique. (b) Optical and SEM images of inkjet-printed prototype IDE sensors. (c) Frequency-dependent change in impedance values for inkjet-printed sensors, before and after iodine adsorption, where DPC stands for drop-casted technique and SC for single-crystal method. For 3-layer-ZIF-70@IDE: (d) A real-time transient measurement of impedance and phase angle at 10 Hz frequency, and (e) cyclic adsorption and desorption data for testing sensor reusability at 4 Hz AC.

Inkjet printing offers several benefits over the commonly used printing techniques, which include superior print resolution, higher control of drop volume, ability to deposit material in multiple layers, scalable, mask less, and additive in nature. To push the study forward toward real-world sensor implementation, we standardized the thickness of the deposited MOF thin film by using piezoelectric-driven drop-on-demand inkjet printing (IP). In this regard, three different prototype sensors were prepared by varying the number of deposited layers (1, 3, and 5 layers) of ZIF-70 as described in the SI (Section 1.2). As can be seen from Fig. 4(b) and Fig. S17, unlike the 1-layer of ZIF-70, the 3-layer sample has completely and uniformly covered the IDE sensor surface with a film thickness of *ca*. 8 μm. In the presence of the I_2 gas, the electrical response from the 1-layer ZIF-70@IDE is insignificant, whereas the 3-layer ZIF-70@IDE showed a record-breaking enhancement of 1.27 millionfold due to its full coverage of the IDE and the minimum film thickness, which allowed the I_2 to adsorb more rapidly and efficiently. This was further supported by two experimental observations: (i) The impedance values of 5-layer ZIF-70@IDE showed a decline, which can be associated with the increased film thickness as compared to the 3-layer ZIF-70@IDE, causing an increase in the adsorption time (see Fig. 4(c)), (ii) A time-dependent electrical response measurements of 3-layer ZIF-70@IDE, which showed a detection time of 3.1 min, revealing its rapid and efficient I_2 adsorption (see Fig. 4(d)). The 3-layer ZIF-70@IDE was also examined for its reversibility through adsorption–desorption test cycles, revealing the remarkably stable electric response of the inkjet-printed films (see Fig. 4(e)). Furthermore, the inkjet-printed MOF film showed an astonishingly high 2.84-billionfold enhancement in the electrical response in direct current (DC), which is considerably higher than the drop-casted and single-crystal MOF@IDE responses discussed above (see Fig. 5(b)). To the best of our knowledge, this value is the highest reported enhancement in the iodine detection sensitivity of both the DC and AC frequencies (see Fig. 5(c) and (d)), signifying a new record in the field of I_2 adsorbent sensors [26–29].

The post-capture phase was analyzed by PXRD, Fourier Transform Infrared Spectroscopy (FTIR), Raman spectroscopy and solid-state UV–visible diffuse reflectance spectroscopy (DRS) (Figs. S19 and S20). The structural integrity remained intact after several sensing experiments confirmed by the unaltered PXRD patterns for both the powder sample and ZIF-70 single crystals, matching the simulated XRD pattern (see Fig. S19(a) and (b)). In the presence of iodine, a shift in the characteristic vibrational bands of ZIF-70 MOF was also observed in the FTIR spectra (see Figs. S19(c) and S20), indicating its ultra-high sensitivity toward the detection of iodine molecules. Unlike the blue shift in the infrared (IR) mode observed at 1174 cm^{-1} (Fig. S20(h)), most of the characteristic peaks exhibit a red shift in peak positions along with peak broadening and a noticeable increase in the intensity of some vibrational bands, which are in line with literature reports [30].

The FTIR spectra were also measured for a time- and temperature-dependent iodine desorbed ZIF-70 MOF to show the reversibility of the peak shift. The results suggest that the iodine confined in the framework is interacting with its surrounding, forming a percolation network thus causing a decline

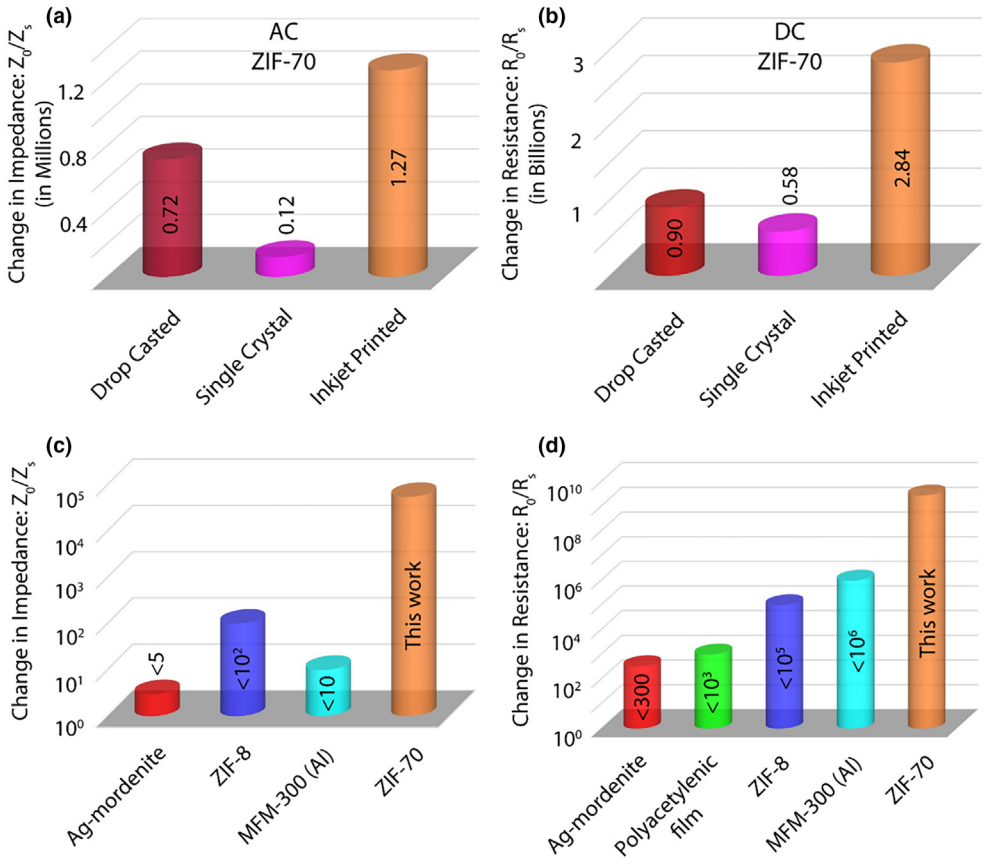

FIGURE 5

A comparative bar plot for the impedance-dependent sensitivity response of drop-casted, single-crystal, and inkjet-printed sensors in (a) 4 Hz alternating current (AC), and (b) direct current (DC). A comparison of the sensor sensitivity between this work and the previously reported IDE-based iodine sensors (data summarized in Table S5) [21–24] for sensing performance in (c) AC at 50 Hz to emulate Great Britain's national grid frequency and (d) at DC.

in the overall impedance. The Raman spectra was also recorded to confirm the existence of the iodine species. Two distinct vibrations were observed for the iodine adsorbed ZIF-70 MOF, which are not present in its pristine state (see Fig. S19(d)). The Raman peak at 112 cm^{-1} was associated with the existence of polyiodide, whereas another peak at 166 cm^{-1} was ascribed to the weakly coordinated iodine [31,32]. The underlying higher area of 166 cm^{-1} peak over its counterpart suggests that iodine exists in the solid form rather than in an ionized form. For bandgap determination, the absorbance spectra for ZIF-70 MOF were measured by DRS and transformed *via* the Kubelka–Munk (KM) method to estimate the optical band gaps. We established the presence of iodine in the pore channels causes a significant reduction in the framework bandgap from 2.78 eV (pristine ZIF-70) to 1.35 eV (I_2@ZIF-70), which can be seen in the inset of Fig. S19(e), further substantiating the observed decrease in the impedance of the prototype MOF@IDEs described above.

Concluding remarks

To accomplish a highly selective and ultra-trace sensitive electrical sensing of iodine gas, we provided a mechanism to identify the key combination of physico-chemical properties in a nanoporous material for the task. The outstanding performance of the prototype MOF@IDE sensors demonstrated here challenges the existing technologies, it brings about a paradigm shift in the field of iodine sensing (see Table S5). We show a reversibly selective and even an ultra-trace ppb-level I_2 gas sensor, effective both at lower (Hz) and higher frequencies (MHz), making it suitable for easy integration into commercial AC electronics. This breakthrough was achieved by optimizing the level of hydrophilicity-hydrophobicity in the MOF material by leveraging the guest–host interaction sites. The mechanism exploits the tunable hydrophilicity-hydrophobicity level in a nanoporous framework, for instance ZIF-70, facilitating an uninterrupted migration of the inbound target gas species through the pores, and the presence of interaction sites as a temporary anchor point to confine gas molecules to allow chemosensing.

In the wider perspective, our work opens the door for the design of smart electrical gas sensors employing optimal hydrophobicity and interaction sites for real-time selective sensing of hazardous and toxic chemicals at ultra-trace levels. This sensing methodology can safeguard against accidents and chemical leaks in numerous industrial and consumer settings, meeting the ever-increasing demand for engineering advanced thin-film sensing technologies with supersensitive target molecule detection.

CRediT authorship contribution statement

Arun S. Babal: Conceptualization, Methodology, Formal analysis, Investigation, Visualization, Writing – original draft, Writing – review & editing. **Samraj Mollick:** Conceptualization, Methodology, Formal analysis, Investigation, Visualization, Writing - original draft, Writing – review & editing. **Waqas Kamal:** Investigation, Methodology, Writing – review & editing. **Steve Elston:** Supervision. **Alfonso A. Castrejón-Pita:** Writing – review & editing, Supervision. **Stephen M. Morris:** Writing – review & editing, Supervision. **Jin-Chong Tan:** Conceptualization, Methodology, Supervision, Funding acquisition, Project administration, Resources, Writing – review & editing.

Declaration of Competing Interest

The authors declare that they have no known competing financial interests or personal relationships that could have appeared to influence the work reported in this paper.

Acknowledgements

A.S.B. thanks the Engineering Science Studentship (EPSRC DTP – Samsung) for supporting this DPhil project. J.C.T. and S.M. thank the ERC Consolidator Grant PROMOFS (grant agreement 771575) for funding the research. J.C.T. acknowledges the EPSRC IAA award (EP/R511742/1) for additional support. W.K. acknowledges the financial support provided by Punjab Education Endowment Fund (PEEF), Pakistan. A.A.C-P was supported by The Royal Society through a University Research Fellowship (URF\R\180016) and the John Fell Fund, Oxford University Press, *via* a Pump-Priming grant (0005176). We thank the Research Complex at Harwell (RCaH) for the provision of TGA, UV-Vis and Raman spectrometers.

Author contributions

A.S.B., S.M. and J.C.T. designed the research. A.S.B. and S.M. conducted the materials synthesis and characterization, and A.S.B. performed the impedance measurements and data analysis, under the supervision of J.C.T. W.K. performed the inkjet printing experiments, under the supervision of A.A.C-P, S.E. and S.M. M. A.S.B. and S.M. wrote the original draft of the manuscript with input from J.C.T. All the authors contributed to the final version of the manuscript.

Competing financial interests

The authors declare that they have no known competing financial interests.

Appendix A. Supplementary data

Supplementary data to this article can be found online at https://doi.org/10.1016/j.mattod.2022.07.001.

References

[1] World Energy Needs and Nuclear Power. World Nuclear Association (2021).
[2] G. Cicia et al., Energy Policy 42 (2012) 59.
[3] P.A. Kharecha, J.E. Hansen, Environ. Sci. Technol. 47 (2013) 4889.
[4] Y.H. Abdelmoaty et al., ACS Appl. Mater. Interfaces 10 (2018) 16049.
[5] A.R. Brosi et al., Phys. Rev. 75 (1949) 1615.
[6] R.R. Edwards, Science 137 (1962) 851.
[7] J. Robbins, A.B. Schneider, Rev. Endocr. Metab. Disord. 1 (2000) 197.
[8] J.E. Ten Hoeve, M.Z. Jacobson, Energy Environ. Sci. 5 (2012) 8743.
[9] W.P. Lustig et al., Chem. Soc. Rev. 46 (2017) 3242.
[10] L.Z. Huang et al., Nanoscale Horiz. 1 (2016) 383.
[11] L.E. Kreno et al., Chem. Rev. 112 (2012) 1105.
[12] H.Y. Yuan et al., Angew. Chem. Int. Ed. 58 (2019) 14089.
[13] H. Deng et al., Science 336 (2012) 1018.
[14] H. Furukawa et al., Science 341 (2013) 1230444.
[15] O.K. Farha et al., Nat. Chem. 2 (2010) 944.
[16] S. Mandal et al., Adv. Funct. Mater. 31 (2020) 1315.
[17] J. Rocha et al., Chem. Soc. Rev. 40 (2011) 926.
[18] J.F. Olorunyomi et al., Mater. Horizons 8 (2021) 2387.
[19] L.T. Zhang et al., Angew. Chem. Int. Ed. 60 (2021) 15192.
[20] E. Aunan et al., Chem. Mater. 33 (2021) 1471.
[21] M.A. Simon et al., Sci. Rep. 9 (2019) 16907.
[22] A.F. Moslein, J.C. Tan, J. Phys. Chem. Lett. 13 (2022) 2838.
[23] R. Banerjee et al., Science 319 (2008) 939.
[24] Y.Q. Hu et al., Chem. Eur. J. 23 (2017) 8409.
[25] T. Hasell et al., J. Am. Chem. Soc. 133 (2011) 14920.
[26] F.N. Dultsev, Sens. Actuator B-Chem. 129 (2008) 171.
[27] L.J. Small, T.M. Nenoff, ACS Appl. Mater. Interfaces 9 (2017) 44649.
[28] L.J. Small et al., ACS Appl. Mater. Interfaces 11 (2019) 27982.
[29] L.J. Small et al., Microporous Mesoporous Mat. 280 (2019) 82.
[30] P. Chen et al., ACS Appl. Mater. Interfaces 12 (2020) 20429.
[31] P.H. Svensson, L. Kloo, Chem. Rev. 103 (2003) 1649.
[32] A. Sen et al., ACS Appl. Mater. Interfaces 13 (2021) 34188.